Received: 19 October 2022 | Revised: 23 November 2022 | Accepted: 17 December 2022

DOI: 10.5185/amlett.2023.031730

OPEN ACCESS

RESEARCH

# Thermionic Emission Induced Current-Voltage behaviour of $GdMnO_3$/Al:ZnO/STO and $GdMnO_3$/ZnO/STO Thin Film Heterostructures

**Pankaj Solanki[1] | Mayur Vala[2] | Sandip V. Bhatt[3] | Dhananjay Dhruv[4] | Bharat Kataria[1]***

[1]Department of Nanoscience and Advanced Materials, Saurashtra University, Rajkot, 360005 India

[2]Department of Physics, Saurashtra University, Rajkot, Gujrat, 360005 India

[3]P.G. Department of Applied and Interdisciplinary Sciences, Sardar Patel University, Vallabh Vidyanagar, Anand, Gujarat, 388120, India

[4]Nathubhai V. Patel College of Pure and Applied Sciences, Charutar Vadya Mandal University, Vallabh Vidyanagar, Anand, Gujarat, 388120, India

***Corresponding author**
E-mail: brkataria22@rediffmail.com

## ABSTRACT

We report the results of studies on the rectifying behaviour and tunnelling conduction in GdMnO3/ZnO/STO and GdMnO3/Al:ZnO/STO thin film heterostructures comprising of p-n junctions fabricated using the Pulsed Laser Deposition (PLD) technique. A structural study using grazing angle mode XRD depicts polycrystalline growth and confirms the phase purity. The AFM micrographs reveals the different grain growth and grain sizes of the prepared thin film heterostructures. Room temperature Raman spectra shows the presence of various vibrational modes in both the thin film heterostructures, the transport studies using I–V measurements at room temperature is explained using various models. The temperature dependent transport studies using I-V measurements at various temperatures reveal the rectifying behaviour and the difference in the I-V behaviour at various temperature can be understood on the basis of interface effect at the junction, which has been attributed to the presence of the various conduction phenomena through the junctions and the change in barrier height with the temperature for both presently studied thin film heterostructures.

## KEYWORDS

Heterostructures, pulsed laser deposition, space charge limited conduction, thermionic emission, barrier height.

## INTRODUCTION

Multiferroics are the important class of materials with various ferroic properties like ferromagnetism, ferroelectricity and ferro-elasticity in single phase which convey temenos interest in research. From discovery of perovskite structure especially rare earth manganites with $AMnO_3$ (A= rare earth elements) have obtained extensive attention, as they possess interesting properties like magnetoresistance, Jahn-Teller distortion, Zener Double Exchange, multiferroic properties [**1-7**]. All these properties can be modified under different external conditions like Heat treatment, pressure, applied fields, irradiation effect, A-site/ B-site doping effect etc. [**8-14**] are induced modification in properties of manganite materials. Manganites can enhance the properties/efficiency of capacitors, transistors, FETs, sensors, memory storage devices etc. [**15-19**]. Manganites attribute the strong relations between spins, lattice, orbitals etc. like fundamental parameters which are responsible for various behaviors such as paramagnetic insulator, ferromagnetic insulator, antiferromagnetic insulator, paramagnetic metallic, ferromagnetic metallic [**15,16**]. To explore this kind of behavior, manganite have been studies in form of polycrystalline bulk materials, composites, thin films, core-cells etc. [**10,15**].

Comparison of polycrystalline bulk and thin films shows a large variation in microstructural as well as different physical properties. Properties of thin films depends on different conditions like choice of substrate, deposition techniques, deposition parameters etc. [**17,18**]. There are several deposition techniques to fabricate thin films such as Spin Coating, Deep Coating, Atomic Layer Deposition (ALD), RF & DC Sputtering, Chemical Vapor Deposition (CVD), Pulse Laser Deposition (PLD) etc.[**18-20**]. Pulsed Laser Deposition (PLD) is most used thin film fabrication technique because as compared to other techniques used in research it provides less stoichiometric distortion. In PLD technique one can control several parameters like substrate temperature, oxygen pressure etc.

There are several reports available for I-V properties of manganite thin films. Khacher *et al.* [**21**] have investigated the temperature dependent I-V behaviour of manganite based thin films, reported that positive magnetoresistance shows strong dependency on the temperature as well as magnetic field. Kataria *et al.* [**14**] have reported the temperature and magnetic field sensitive resistivity behaviour with SHI irradiation. Temperature plays important role in modification of physical properties of manganite-based structures. Ravalia *et al.* [**13**] investigate the variation in barrier height of manganite based thin films with temperature. Solanki *et al.* [**22**] reported the light dependency of I-V behaviour of LCMO/Si p-n junction and the thickness effect on charge conduction. Various responsible charge conduction mechanism for temperature dependent I-V behaviour have studied by Gadani *et al.* [**23**].

Among the all-manganite structures, $GdMnO_3$ based structures are not far studied as compared to other manganites. There are few reports are available for single layer $GdMnO_3$ thin films. Andreev *et al.* [**24**] have fabricated $GdMnO_3/NdGaO_3$ thin film to investigate the magnetic phase transition. Romaguera *et al.* [**25**] have studied the Raman and magnetic properties of $GdMnO_3$ thin film grown on Pt substrate. Negi *et al.* [**26**] reported the weal ferromagnetic phase at lower temperature in PLD grown $GdMnO_3/Si$ thin film. Hitherto no reports available for $GdMnO_3$ based multilayers/heterostructures.

A noticeable amount of work has carrier out to study the I-V characteristic and resistive switching behavior of rhombohedral $BiFeO_3/ZnO$ based heterostructures [**27-30**], $GdMnO_3$/Al:ZnO/SNTO heterostructure exhibits a good resistive switching behaviour [**31**], it will be very interesting to study the I-V behaviour and the effect of temperature on the electrical transport characteristics of the $GdMnO_3/ZnO$ (Al:ZnO) bilayers fabricated on $SrTiO_3$ substrate.

In present communication, the results of the studies on temperature effect on transport behaviour have been reported for $GdMnO_3$/Al:ZnO/$SrTiO_3$ and $GdMnO_3/ZnO/SrTiO_3$ manganite-based bilayer thin film heterostructures. Herein, manganite-semiconductor structures were fabricated using Pulsed Laser Deposition (PLD) system. We investigated the structural, topographical, vibrational and transport properties of $GdMnO_3$/Al:ZnO/$SrTiO_3$ and $GdMnO_3/ZnO/SrTiO_3$ bilayer thin films, especially focused on the transport behaviour of both films. To understand transport mechanism some theoretical models have been used.

## EXPERIMENTAL DETAILS

Firstly, all the required targets ($GdMnO_3$, ZnO and 2% Al doped ZnO) were prepared using high temperature SSR route. Then, Al:ZnO/ZnO semiconductor layers were fabricated on *(100)* single crystalline $SrTiO_3$ substrate, then after masking $GdMnO_3$ manganite layer was fabricated on Al:ZnO/$SrTiO_3$ and ZnO/$SrTiO_3$ films using Pulsed Laser Deposition system (parameters: laser energy: -~ 225 mJ and ~240 mJ, Pulse rate: - 5 Hz, substrate temperature: - 800°C, partial oxygen pressure: - ~ 250 mTarr and ~75 mTarr for $GdMnO_3$ and ZnO/Al-ZnO layers respectively). The X-ray Diffraction pattern were taken using Cu Kα radiation for structural analysis of prepared thin films. For better understanding phase identification, X-ray Diffraction Pattern were taken with grazing angle mode. For topographical analysis, Atomic Force Micrographs were taken using Nanoscop V-3100 (Bruker). For vibrational mode identification, the Raman spectra were obtained over a range from 100 $cm^{-1}$ to 1200 $cm^{-1}$ with a spectral resolution of 1 $cm^{-1}$ at an excitation wavelength of 785 nm, using A Renishaw confocal micro-Raman spectrometer with a liquid-nitrogen-cooled charge-coupled device was used to analyze the backscattered light. The laser spot power incident on the sample was kept below 5mW to avoid any sample heating. The temperature dependent Current-Voltage (I-V) measurements were taken to investigate the transport behaviour of all fabricated films using the Keithley Source Metter (Model- 4200SCS). Current-Voltage (I-V) measurements were taken using the DC two probe method with Current Perpendicular to plane (CPP) mode in voltage range of -5 V to +5 V for both heterostructures for this Ag (silver) patches formed on the surface of both the GMO manganite layer and the AZO/ZO layer.

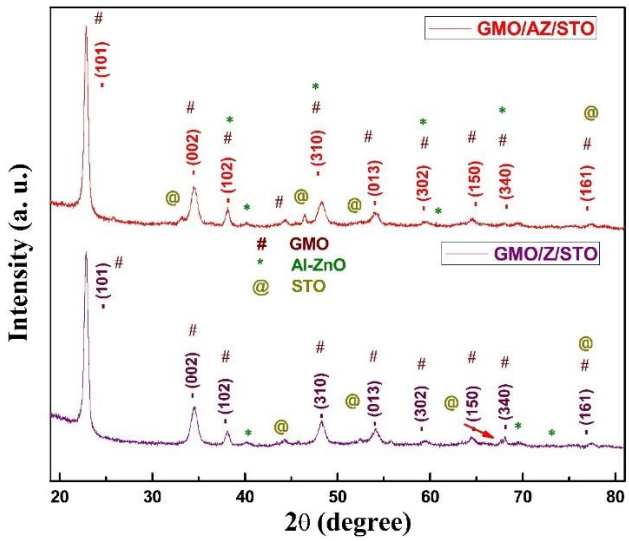


**Fig. 1.** X-ray diffraction patterns for polycrystalline (a) $GdMnO_3$/Al:ZnO/$SrTiO_3$ and (b) $GdMnO_3/ZnO/SrTiO_3$ thin film heterostructures taken at 1.5° grazing angle.

## RESULTS AND DISCUSSIONS

### *X-ray Diffraction (XRD) Measurements*

**Fig. 1** displays the X-ray diffraction patterns for $GdMnO_3$/Al:ZnO/$SrTiO_3$ (GMO/AZ/STO) and $GdMnO_3/ZnO/SrTiO_3$(GMO/Z/STO). X-ray Diffraction

pattern taken at 1.5º grazing angle to confirm the polycrystalline growth of all proposed layers. The X-ray Diffraction patterns confirm the orthorhombic *(Pnma)* growth of $GdMnO_3$ and wurtzite hexagonal phase growth of Al:ZnO and ZnO layers. The tensile strain (+0.07%) and compressive strain (-0.15%) were present at interface of $GdMnO_3$/ Al:ZnO and $GdMnO_3$/ZnO bilayers respectively. The lattice mismatch/strain calculated using following relation,

$$\delta(\%) = \left[\frac{(d_{substrate} - d_{film})}{d_{film}}\right] \times 100 \quad (1)$$

***Atomic Force Microscopy (AFM) measurements***

Atomic Force Microscopy (AFM) is the technique which helps to study the surface topography of thin films. **Fig. 2 (a-h)** reveals the surface topographic images with 3-dimentional (**Fig. 2(a)** & **Fig. 2(e)**) and 2-dimentional (**Fig. 2(b)** & **Fig. 2(f)**) view as well as surface profile (**Fig. 2(c)** & **Fig. 2(g)**) and RMS Roughness (**Fig. 2(d)** & **Fig. 2(h)**) studies for prepared GMO/AZ/STO and GMO/Z/STO thin films respectively.

Island type growth for both the strictures is confirmed from the 3D view of surface, GMO/AZ/STO possesses large islands as compared to GMO/Z/STO film. Also, Z-axis scale bar reveals the large difference in grain height for GMO/AZ/STO (~236 nm) and GMO/Z/STO (~70.8 nm) thin films. Surface profile suggests homogeneous grain growth with ~1.93 µm and ~172 nm average grain size for both films respectively as well as RMS roughness found to be ~ 36.7075 (GMO/AZ/STO) and ~ 7.1297 (GMO/Z/STO) respectively. The difference in microstructure of both the layered films helps to understand the difference in Current-Voltage relation of both the structures.

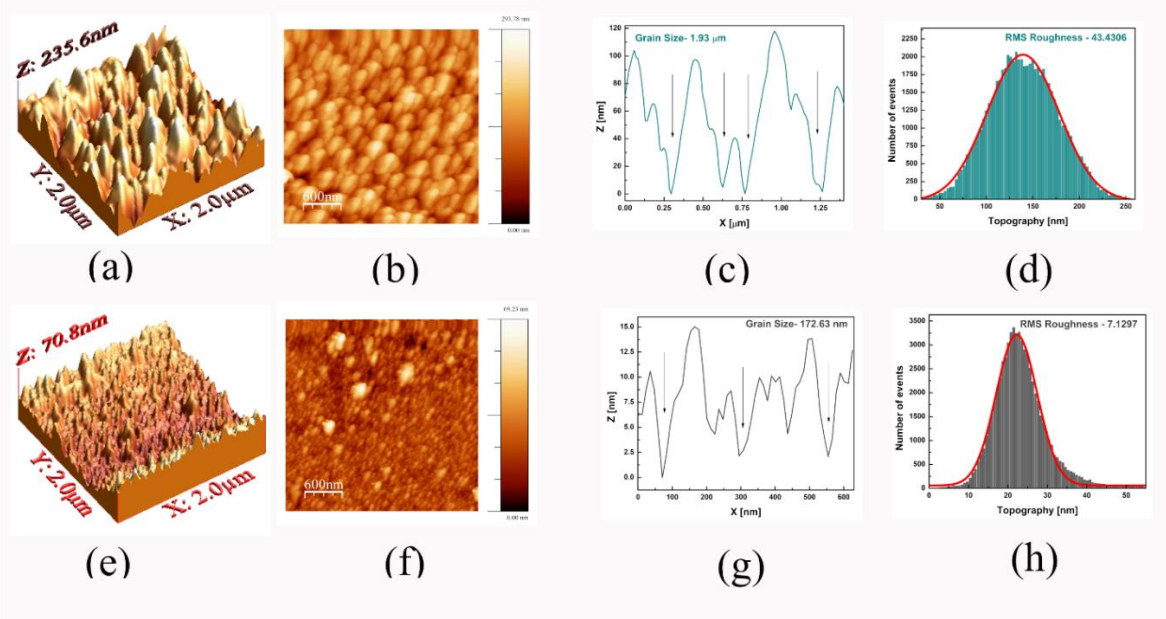


**Fig. 2**. AFM Images for GMO/AZ/SNTO and GMO/Z/SNTO heterostructures; (a & e) 2D view surface topography, (b & f) 3D view of surface topography with Z- axis scale bar, (c & g) granular (surface) profile for randomly selected grains, (d & h) average RMS roughness analysis respectively.

***Raman measurements***

Raman spectroscopy studies related vibrations of atomic bonds present in structure, all vibrations are associate with significant phonon modes. For the orthorhombic structure, 60 phonon vibrational modes are associated with Γ-point among them 24 modes (*7A g+5B 1g+7B 2g+5B 3g*) Raman active, 25 modes (*9B 1u+7B 2u+9B 3u*) infrared active, 8 modes (*8A u*) silent mode, and 3 are acoustic modes (*3B 1u+B 2u+B 3u*) respectively. Two $MnO_6$ octahedra were found in the $GdMnO_3$ crystal lattice, as well as two axial O2 and four equatorial O1 ions on the y-axis. The xy-plane and y-axis are parallel to the Mn-O1 and Mn-O2 bonds, respectively.

**Fig. 3(a)** and **Fig. 3(b)** represents the typical room temperature Raman spectra for GMO/AZ/STO and GMO/Z/STO thin films respectively. The Raman shifts were identified using the Lorentz function fitted on experimentally observed spectrum. As shown in **Fig. 3(a)** and **Fig. 3(b)**, Raman spectra reveals strong Raman Shifts 245.48 $cm^{-1}$, 273.98 $cm^{-1}$, 374.98 $cm^{-1}$,415.33 $cm^{-1}$, 486.56 $cm^{-1}$, 504.41 $cm^{-1}$, 616.06 $cm^{-1}$, 679.01 $cm^{-1}$ and 728.89 $cm^{-1}$ as well as 243.10 $cm^{-1}$, 275.17 $cm^{-1}$, 374.98 $cm^{-1}$, 411.76 $cm^{-1}$, 486.59 $cm^{-1}$, 505.60 $cm^{-1}$, 618.43 $cm^{-1}$, 677.82 $cm^{-1}$ and 726.52 $cm^{-1}$ for GMO/AZ/STO and GMO/Z/STO thin films respectively, which shows significance with previously reported data [**32-34**]. The majority Raman shifts corresponds with

$GdMnO_3$, only 245.48 $cm^{-1}$, 679.01 $cm^{-1}$ (for GMO/AZ/STO) and 243.10 $cm^{-1}$, 677.82 $cm^{-1}$ (for GMO/Z/STO) Raman Shifts are related with lattice-substrate interaction. From the close observation of the Raman spectra, one finds the five Raman active modes especially four $A_g$ and one $B_{2g}$ which is associated with $MnO_6$ octahedra present in $GdMnO_3$.

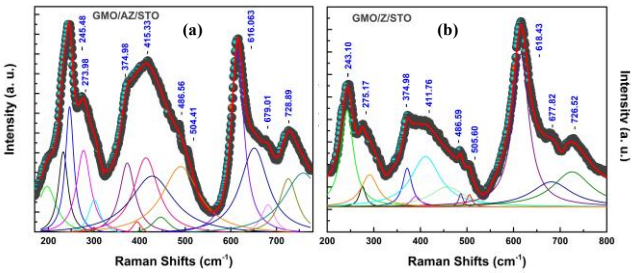


**Fig. 3.** Typical Micro-Raman Spectra for (a) GMO/AZ/STO and (b) GMO/Z/STO thin film heterostructures taken at room temperature.

The $A_g$ symmetry which corresponds to tilting of $MnO_6$ octahedra reveals by 273.98 $cm^{-1}$ and 275.17 $cm^{-1}$. The Raman shift at 374.98 $cm^{-1}$ reveals the $A_g$ mode associated with the out of phase *x* rotations of $MnO_6$. The $A_g$ mode having $MnO_6$ bending and O2 anti-stretching were located at 486.56 $cm^{-1}$ and 504.41 $cm^{-1}$ as well as 486.59 $cm^{-1}$ and 505.60 $cm^{-1}$ respectively. The $B_{2g}$ mode with the symmetric stretching mode involving the equatorial oxygen atoms is associated with the prominent band at 616.06 $cm^{-1}$ and 618.43 $cm^{-1}$ respectively.

The other modes, at 245.48 $cm^{-1}$, 679.01 $cm^{-1}$ (for GMO/AZ/STO) and 243.10 $cm^{-1}$, 677.82 $cm^{-1}$ (for GMO/Z/STO), possibly represent interactions between the $GdMnO_3$ films and the $SrTiO_3$ substrate [**25,34-36**]. Moreover, the Raman shift at 728.89 $cm^{-1}$ as well as 726.52 $cm^{-1}$ can be attributed to longitudinal optical (LO) branches of $SrTiO_3$ substrate [**37**]. It is observed that most Raman spectral features are approximately identical, although the intensity decreases. The Raman spectra of $GdMnO_3$/ZnO bilayers exhibit a broad band in the 380-480 $cm^{-1}$ region, which may attributed to the emergence of the $E_2^{high}$ mode of Wurtzite ZnO structure [**38**].

***Current-Voltage (I-V) measurements***

Before delving into the transport studies, it is worth noting that Ag (silver) patches formed on the surface of both the GMO manganite layer and the AZO/ZO layers. In this study, these Ag patches served as electrodes for the Current-Voltage (I-V) behavior. During the experiment, these patches were made with the same size and thickness. The effects of the ohmic contact between the Ag electrode and all layers (for both films) on the transport properties of both films will be the same when analyzing the transport measurement results. In this case, changes in the results of transport characterizations are regarded as film behavior rather than any effective ohmic contact.

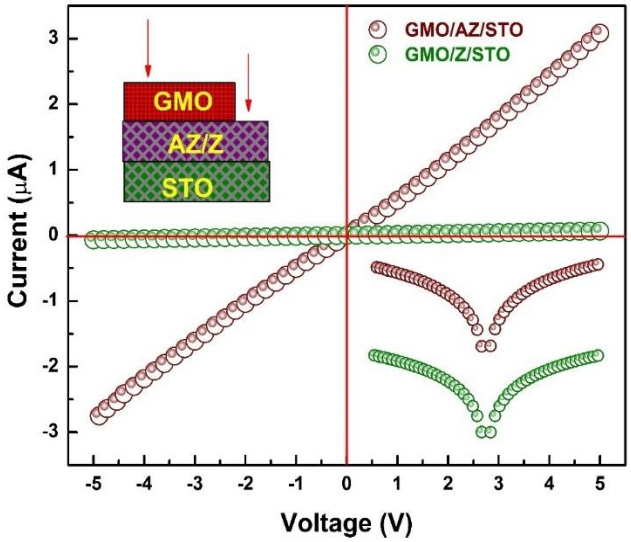


**Fig. 4.** Room temperature Current-Voltage (I-V) characteristics for GMO/AZ/STO and GMO/Z/STO thin film. (Insets: CPP geometry and Semi-logarithmic scale view)

To understand the transport behaviour across the Ag-GMO/AZ_Z-Ag interfaces of prepared GMO/AZ_Z/STO thin films, Current-Voltage (I-V) measurements were taken using the DC two probe method with Current Perpendicular to Plane (CPP) mode at room temperature. Room temperature I-V behaviour in range of -5 V to +5 V for both films are shown in Figure 4. The insets of Figure 4 represent schematic diagram of CPP mode as well as logarithmic plot of I-V behaviour of prepared films.

**Fig. 4** reveals that both Thin film heterostructures possess rectifying behaviour with rectification ratio ($I_F/I_R$) of ~1.12 and ~0.98 at 5 V respectively, indicating majority charge carriers flow from semiconductor layer to manganite layer [**39**]. Herein one can consider that there is no major role of $GdMnO_3$ in charge transport behaviour in particular study deciding the rectification. Also, the filamentary paths created at the interface, which creates tunneling effect at the interface, are responsible for the increment in current and the rectification [**31**]. From **Fig. 4**, it is observed that GMO/AZ/STO film contains higher value of current compared to that in GMO/Z/STO, because Al:ZnO contains higher carrier concentration as compared to ZnO and for present case the charge carries are flowing from Al:ZnO and ZnO layer to GMO layer of GMO/AZ/STO and GMO/Z/STO films respectively which may be responsible for the high value of current for GMO/AZ/STO thin film heterostructures. Another factor affecting the charge on rectifying ratio is the microstructure presented in **Fig. 2**, in which the GMO layer in GMO/Z/STO films is having larger grains and hence smaller number of grain boundaries offering the small resistance to the current, whereas the smaller grains and larger number of grain boundaries offer comparatively large resistance for the case of GMO/Z/STO layered thin films.

In context to understand the chare transport mechanism responsible for the observed room temperature Current-Voltage (I-V) behavior across the GMO/AZ and GMO/Z interface, the experimental data were fitted to various theoretical models, namely,

(i) Fowler-Nordheim (FN) Tunneling [**40**]

$$J_{FN} = AE^2 exp\left(\frac{-B^2\sqrt{\emptyset^3}}{\mathrm{E}}\right) \quad (2)$$

where, *A* and *B* are constant; E is the applied electric field and ∅ is potential barrier height.

(ii) Poole-Frenkel (PF) Emission [**41**]

$$J_{PF} = BE\ exp\left(\frac{-\mathrm{E}_1-\sqrt{\mathrm{q}^3\frac{\mathrm{E}}{4\pi\varepsilon_0\mathrm{k}}}}{\mathrm{K_B T}}\right) \quad (3)$$

where *B* is a constant, *E* is the electric field applied to interfaces, $E_1$ is the trap ionization energy, *q* is electron charge $K_B$ is Boltzmann's Constant, T is absolute temperature, $\varepsilon_0$ is the permittivity of free space and *k* is the optical dielectric constant of heterostructure.

(iii) Schottky Emission/Barrier [**42**],

$$J_{Schottky} = AT^2 exp\left(\frac{\emptyset-\sqrt{\mathrm{q}^3\frac{\mathrm{E}}{4\pi\varepsilon_0\mathrm{k}}}}{\mathrm{K_B T}}\right) \quad (4)$$

where, *A* is a constant; *T* is absolute temperature; *E* is the electric field; $k_B$ is Boltzmann's constant; ∅ is the barrier height; $\varepsilon_0$ is the permittivity of free space and *k* is the optical dielectric permittivity of thin film

(iv) Space Charge Limited (SCL) Conduction [**42**],

$$J_{SCLC} = \frac{9\mu\varepsilon_0 kV^2\theta}{8d_s^3}\exp\left[0.891\beta\left(\frac{V}{d_s}\right)^{1/2}\right] \quad (5)$$

where, $\mu$ is the mobility of electron, *k* is the permittivity, $\varepsilon_0$ is permittivity of free space, $\theta$ is free to total carrier density ratio, $d_s$ is thickness of film,

(v) Simmons Model [**42**] etc.

$$I = (\sigma \times V) + (k \times V^n) \quad (6)$$

where, $\sigma$ represents the conductivity, $k$ represents the constant which depending upon the barrier at interface.

Our obtained data best fits to two different theoretical models namely (i) Space Charge Limited (SCL) conduction and (ii) Simmons model. **Fig. 5(a)** & **Fig. 5(c)** show the Space Charge Limited Conduction (SCLC) fittings for Forward and Reverse bias of GMO/AZ/STO and GMO/Z/STO Thin film heterostructures respectively. Space Charge Limited Conduction (SCLC) model fitted for full voltage range which reveals that GMO/AZ and GMO/Z interfaces shows the ohmic behavior. To support the Space Charge Limited Conduction mechanism, linear fit for *dV/d (ln I) vs I* were performed. **Fig. 5(b)** & **Fig. 5(d)** provide the value of series resistance present at the interface of the film. The series resistance is dominant factor for the ohmic behavior of any junction [**43**]. The fitting parameters are tabulated in **Table 1**.

**Fig. 5(e)** and **Fig. 5(f)** show the Simmons model fitting for the GMO/AZ/STO and GMO/Z/STO thin filmns respectively. Fitting the Simmons moded on nonlinear curve, provides value of n which is associate with the different posible charge transport mechanism. If the value of n ≥ 0.6 then charge conduction can be considerad tunneling through the disorderad metalic oxides. For the n = 1.33, quasiparticle tunneling via the pairs localized states. The stron spin-flip scattering at the insulating barries attirbute for chare conduction if n > 1.4. When n=2, direct tunneling of charge cerries across the barries causes the tunneling [**42**]. In present cases, obtained value of n ( 0.72 ≤ n ≤ 1.33) indicate that the charge condution is controlled by disordered metalic oxide (at interface due to lattice mismatch). Value of n is tabulated in **Table 1**.

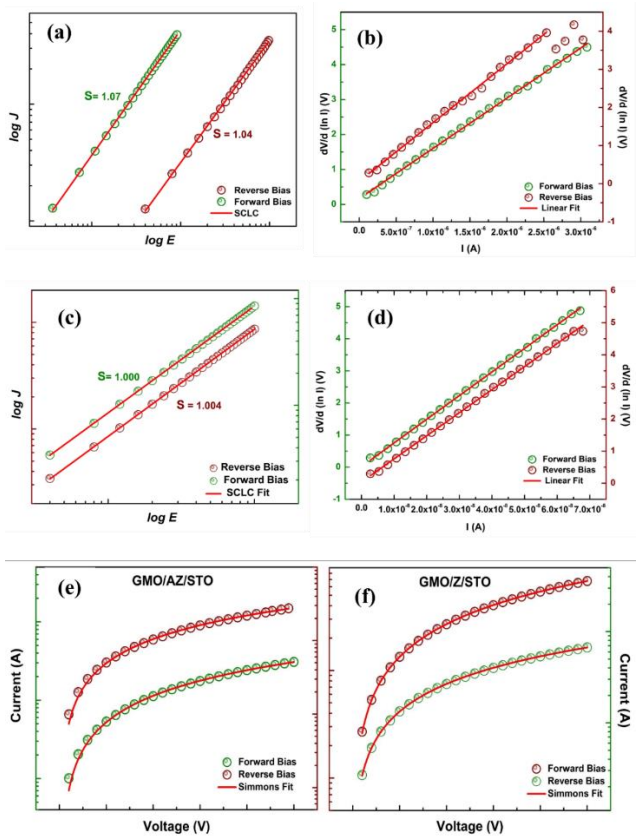


**Fig. 5.** (a) & (c) Space Charge Limited (SCL) conduction, (b) & (d) Liner fits of *dV/d(lnI) vs I* linear, (e) & (f) Simmons model fittings to room temperature Current-Voltage (I-V) characteristics for GMO/AZ/STO and GMO/Z/STO thin film heterostructures respectively.

**Table 1.** Fitting parameters obtained from *dV/d(lnI) vs I* linear fitting and Simmons model.

| | | *dV/d(lnI) vs I* graph | | Simmons Model Fitting |
|---|---|---|---|---|
| | | Ideality Factor ($\eta$) | Series Resistance (Ω) | n |
| GMO/AZ/STO | FB | 0.16 | 1.43 | 1.31 |
| | RB | 1.10 | 1.68 | 1.33 |
| GMO/Z/STO | FB | 0.02 | $7.36 \times 10^7$ | 0.72 |
| | RB | 0.03 | $7.18\times 10^7$ | 0.84 |

To understand the temperature effect on charge conduction at insulating- semiconductor interface, the temperature dependent Current-Voltage (I-V) measurements are being carried out. Figure 6 (a) and (b) show the I-V behavior obtained at various temperature (50ºC, 100ºC & 150ºC) for GMO/AZ/STO and GMO/Z/STO thin film heterostructures respectively and insets of **Fig. 6(a)** & **Fig. 6(b)** shows current variation at lower voltage. As shown in **Fig. 6(a)** & **Fig. 6(b)**, as temperature increases the value of current is increases for both bilayers. The increment in current with temperature can be describes in two different ways, (i) The thermal injection charge carries [**39**] and (ii) internal annealing [**44**] at the interface respectively.

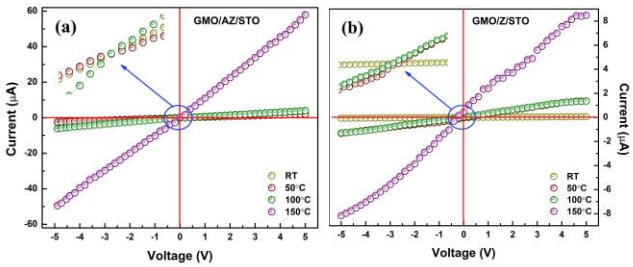


**Fig. 6.** Temperature dependent Current-Voltage (I-V) characteristics for (a) GMO/AZ/STO (b) GMO/Z/STO thin film heterostructures (at 50ºC, 100ºC & 150ºC). (Inset: enlarged view of lower voltage region).

The thermal injection of charge carrier can be predicted because of the partial substitution of $Zn^{+2}$ by $Mn^{+3}$ in GMO/AZ and GMO/Z lattices of the thin film heterostructures which increase the carrier concentration at the interface as temperature increases [**45**]. Khushal *et al.* [**46**] also reported the partial substitution or effective diffusion of $Zn^{+2}$ in LSMO manganite at interface that results in $La_{0.7}Sr_{0.3}Mn_{1-y}Zn_yO_3$ form of stoichiometry. In thin films, the electrical resistance strongly obeys the annealing temperature in context of grain boundaries. The increment in temperature causes the partial annealing at the interfaces which causes decrement in grain boundaries, resulting observed increment in current due to increment in crystallinity which decrease the electrical resistance of thin films at interfaces. To convey the fact of temperature effect on charge conduction, the modified Thermionic Emission model were fitted for I-V data collected at different temperature (50ºC, 100ºC & 150ºC) using the relation,

$$I = AT^2 exp\left(-\left[\frac{\left\{\Phi_B - q\left(\frac{qV}{4\pi\varepsilon d}\right)^{1/2}\right\}}{KT}\right]\right) \quad (7)$$

where $\Phi_B$ is the barrier height, $q$ is the charge of carrier, $\varepsilon$ is the permittivity of material, $d$ is the barrier width and $K$ is Boltzmann constant. **Fig. 7(a)** and **Fig. 7(b)** represent the theoretically fitted experimental I-V data at different temperature (50ºC, 100ºC & 150ºC). Form the fitting, there is a decrement in $\Phi_B$ value (tabulated in **Table 2**) with increment in temperature for both thin film heterostructures, suggesting that with temperature crystallinity increases (decreasing lattice mismatch) at the interface which in turn increase the charge conduction due to the thermal excitation effect on the charge carriers [**47**]. In other words, the interface of heterostructures is modified with temperature and the discontinuity at manganite-semiconductor interface decreases [**48**].

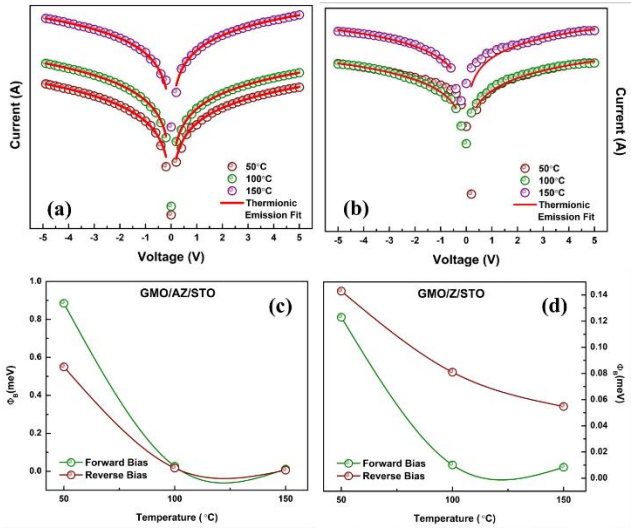


**Fig. 7.** Thermionic emission model fitting for Temperature Dependent Current-Voltage (I-V) characteristics for (a) GMO/AZ/STO and (b) GMO/Z/STO thin film heterostructures (at 50ºC, 100ºC & 150ºC). Variation of barrier height with temperature for (c) GMO/AZ/STO and (d) GMO/Z/STO thin film heterostructures.

**Table 2.** Fitting parameters from Thermionic emission model.

| | Temperature | | Thermionic Model $\Phi_B$(eV) |
|---|---|---|---|
| GMO/AZ/STO | 50 ºC | FB | $8.85 \times 10^{-4}$ |
| | | RB | $5.50 \times 10^{-4}$ |
| | 100ºC | FB | $2.59 \times 10^{-5}$ |
| | | RB | $1.70 \times 10^{-5}$ |
| | 150ºC | FB | $1.16 \times 10^{-5}$ |
| | | RB | $5.85 \times 10^{-6}$ |
| GMO/Z/STO | 50 ºC | FB | $1.23 \times 10^{-4}$ |
| | | RB | $1.43 \times 10^{-4}$ |
| | 100ºC | FB | $1.01 \times 10^{-5}$ |
| | | RB | $8.10 \times 10^{-5}$ |
| | 150ºC | FB | $8.35 \times 10^{-6}$ |
| | | RB | $5.48 \times 10^{-5}$ |

## CONCLUSION

In conclusion, we successfully fabricated the polycrystalline GMO/AZ/STO and GMO/Z/STO thin film heterostructures using Pulsed Laser Deposition System. The growth of orthorhombic GMO layer and Wurtzite hexagonal Al:ZnO/ ZnO structure was confirmed by X-ray diffraction patterns. The AFM images reveals the topographical behaviour of prepared films. From AFM analysis, found that GMO/AZ/STO film possess larger grain size as compared to GMO/Z/STO film. The Raman spectra confirms the bending and stretching of $MnO_6$ octahedra presence in $GdMnO_3$ layer. The transport

behaviour of prepared films understood with Current-Voltage (I-V) behaviour. Both films show rectifying behaviour at room temperature. From the I-V measurements one found that GMO/AZ/STO shows higher value of current because it contains more charge carriers as compared to GMO/Z/STO films. For better understanding of room temperature conduction mechanism, Space Charge Limited Conduction (SCLC) and Simmons model were fitted. SCLC fitting reveals the ohmic behaviour of prepared films which rather supported by *dV/d(lnI) vs I* graphs and provides value of series resistance for both films. Simmons model suggested that charge conduction attributed with tunneling though disordered metallic oxides. Temperature dependent I-V behaviour shows that increment in temperature increases current and shows rectifying nature at high temperature. The increment in current at comparatively high temperatures attributed as partial annealing effect at the interface. Thermionic emission model was employed to understand the temperature effect at interface, reveals that with increasing temperature barrier height decreases, promoting the charge conduction. The obtained results show that interfacial coupling between manganite and semiconductor materials could be controlled by applied voltages and temperatures that immensely improves the promising applications of manganite/semiconductor heterostructures in multifunctional electronic devices.

## ACKNOWLEDGMENTS

This work was financially supported by DST-SERB, New Delhi project (File No. EEQ/2019/000297). The experimental facilities provided by Dr. Sunil Chaki, P. G. Department of Physics, S. P. University, Vallabh Vidyanagar are gratefully acknowledged.

## DATA AVAILABILITY

The datasets generated during and/or analysed during the current study are available from the corresponding author on reasonable request.

## REFERENCES

1. Tomuta, D.; Ramakrishnan, S.; Nieuwenhuys, G.; Mydosh, J.; The magnetic susceptibility, specific heat and dielectric constant of hexagonal $YMnO_3$, $LuMnO_3$ and $ScMnO_3$, *Journal of Physics: Condensed Matter.*, **2001**, *13*, 4543.
2. Rao, C.N.R.; Raveau, B.; Colossal magnetoresistance, charge ordering and related properties of manganese oxides, *World Scientific*, **1998**.
3. Tokura, Y.; Tomioka, Y.; Kuwahara, H.; Asamitsu, A.; Moritomo, Y.; Kasai, M.; Origins of colossal magnetoresistance in perovskite-type manganese oxides, *Journal of Applied Physics.*, **1996**, *79*, 5288-5291.
4. Hwang, H.; Cheong, S.; Radaelli, P.; Marezio, M.; Batlogg, B.; Lattice Effects on the Magnetoresistance in Doped LaMn O 3, *Physical Review Letters.*, **1995**, *75*, 914.
5. von Helmolt, R.; Wecker, J.; Holzapfel, B.; Schultz, L.; Samwer, K.; Giant negative magnetoresistance in perovskitelike La 2/3 Ba 1/3 MnO x ferromagnetic films, *Physical Review Letters*, **1993**, *71*, 2331.
6. Huang, Z.; Cao, Y.; Sun, Y.; Xue, Y.; Chu, C.; Coupling between the ferroelectric and antiferromagnetic orders in YMnO 3, *Physical Review B.*, **1997**, *56*, 2623.
7. Kimura, T.; Goto, T.; Shintani, H.; Ishizaka, K.; Arima, T.; Tokura, Y.; Magnetic control of ferroelectric polarization, *Nature*, **2003**, 426, 55-58.
8. Solanki, P.; Solanki, P.S.; Shah, N.A.; Kataria, B.R.; *International Journal of Scientific Research and Reviews*, **2018**, 6.
9. Wang, L.; Zhang, X.; Pressure dependence of phase transition in undoped LaMnO3, *Physica C: Superconductivity*, **2002**, *371*, 330-338.
10. Doshi, R.; Solanki, P.; Krishna, P.; Das, A.; Kuberkar, D.; Magnetic phase coexistence in $Tb^{+3}$-and $Sr^{+2}$-doped $La_{0.7}Ca_{0.3}MnO_3$ manganite: A temperature-dependent neutron diffraction study, *Journal of Magnetism and Magnetic Materials*, **2009**, 321, 3285–3289.
11. Doshi, R.; Solanki, P.; Khachar, U.; Kuberkar, D.; Krishna, P.; Banerjee, A.; Chaddah, P.; First order paramagnetic–ferromagnetic phase transition in $Tb^{3+}$ doped $La_{0.5}Ca_{0.5}MnO_3$ manganite, *Physica B: Condensed Matter*, **2011**, *406*, 4031-4034.
12. Khachar, U.; Solanki, P.; Choudhary, R.; Phase, D.; Kuberkar, D.; Positive MR and large temperature–field sensitivity in manganite based heterostructures, *Journal of Materials Science & Technology*, **2013**, *29*, 989-994.
13. Solanki, P.; Khachar, U.; Vagadia, M.; Ravalia, A.; Katba, S.; Kuberkar, D.; Electroresistance and field effect studies on manganite based heterostructure, *Journal of Applied Physics*, **2015**, *117*, 145306.
14. Kataria, B.; Solanki, P.; Khachar, U.; Vagadia, M.; Ravalia, A.; Keshvani, M.; Trivedi, P.; Venkateshwarlu, D.; Ganesan, V.; Asokan, K.; Role of strain and microstructure in chemical solution deposited $La_{0.7}Pb_{0.3}MnO_3$ manganite films: thickness dependent swift heavy ions irradiation studies, *Radiation Physics and Chemistry*, **2013**, *85*, 173-178.
15. Dhruv, D.; Joshi, Z.; Kansara, S.; Pandya, D.; Markna, J.; Asokan, K.; Solanki, P.; Kuberkar, D.; Shah, N.; Temperature-dependent I–V and C–V characteristics of chemically-grown $Y_{0.95}Ca_{0.05}MnO_3$/Si thin films, *Materials Research Express*, **2016**, 3, 036402.
16. Solanki, P.; Vala, M.; Siddhapura, P.; Bhatt, S.V.; Ranjan, M.; Kataria, B.; Structural, Electrical and Magnetic properties of orthorhombic $GdMn_{1-X}Ni_XO_3$ ($0 \leq x \leq 0.1$): Influence of Ni doping, *Journal of Magnetism and Magnetic Materials*, **2022**, 170102.
17. Parmar, R.; Markna, J.; Solanki, P.; Doshi, R.; Vachhani, P.; Kuberkar, D.; Grain Size Dependent Transport and Magnetoresistance Behavior of Chemical Solution Deposition Grown Nanostructured $La_{0.7}Sr_{0.3}MnO_3$ Manganite Films, *Journal of Nanoscience and Nanotechnology*, **2008**, *8*, 4146-4151.
18. Haghiri-Gosnet, A.; Renard, J.; CMR manganites: physics, thin films and devices, *Journal of Physics D: Applied Physics*, **2003**, 36, R127.
19. Shang, D.; Wang, Q.; Chen, L.; Dong, R.; Li, X.; Zhang, W.; Effect of carrier trapping on the hysteretic current-voltage characteristics in Ag/ $La_{0.7}Ca_{0.3}MnO_3$/ Pt heterostructures, *Physical Review B.*, **2006**, *73*, 245427.
20. Zeng, X.; Wong, H.; Epitaxial growth of single-crystal (La, Ca) $MnO_3$ thin films, *Applied Physics Letters*, **1995**, *66*, 3371-3373.
21. Khachar, U.; Solanki, P.; Choudhary, R.; Phase, D.; Ganesan, V.; Kuberkar, D.; Current–voltage characteristics of PLD grown manganite based $ZnO/La_{0.5}Pr_{0.2}Sr_{0.3}MnO_3/SrNb_{0.002}Ti_{0.998}O_3$ thin film heterostructure, *Solid State Communications*, **2012**, 152, 34-37.
22. Solanki, P.; Lakhani, P.; Ravalia, A.; Kataria, B.; Effect of Incident Light on Transport Properties of Pulsed Laser Deposited Manganite Thin Films, *Advanced Materials Letters*, **2020**, *11*.
23. Gadani, K.; Dhruv, D.; Joshi, Z.; Boricha, H.; Rathod, K.; Keshvani, M.; Shah, N.; Solanki, P.; Transport properties and electroresistance of a manganite based heterostructure: role of the manganite–manganite interface, *Physical Chemistry Chemical Physics*, **2016**, *18*, 17740-17749.
24. Andreev, N.; Chichkov, V.; Sviridova, T.; Tabachkova, N.; Volodin, A.; Van Haesendonck, C.; Mukovskii, Ya; Growth, structure, surface topography and magnetic properties of $GdMnO_3$ multiferroic epitaxial thin films, EPJ Web of Conferences, **2013**, *40*, 15014.
25. Romaguera-Barcelay, Y.; Moreira, J.A.; Almeida, A.; Araújo, J.P.; de la Cruz, J.P.; Dimensional effects on the structure and magnetic properties of GdMnO3 thin films, *Materials Letters*, **2012**, 70, 167-170.
26. Negi, P.; Dixit, G.; Agrawal, H.M.; Srivastava, R.C.; Structural, Optical and Magnetic Properties of Multiferroic $GdMnO_3$ Nanoparticles, *J. Supercond Nov Magn.*, **2013**, 26, 1611-1615.

27. Shrimali, V.; Gadani, K.; Rajyaguru, B.; Dadhich, H.; Pachchigar, V.; Dhruv, D.; Joshi, A.; Ranjan, M.; Solanki, P.; Shah, N.; Effects of annealing treatment on microstructure, electrical and magnetodielectric properties of $BiFe_{0.98}Co_{0.02}O_3$/Al–doped ZnO layered thin films prepared by chemical solution deposition, *Journal of Alloys and Compounds*, **2020**, 827, 154278.
28. Xu, J.; Jia, Z.; Zhang, N.; Ren, T.; Influence of La and Mn dopants on the current-voltage characteristics of $BiFeO_3$ /ZnO heterojunction, *Journal of Applied Physics*, **2012**, *111*, 074101.
29. Zheng, P.; Sun, B.; Chen, Y.; Elshekh, H.; Yu, T.; Mao, S.; Zhu, S.; Wang, H.; Zhao, Y.; Yu, Z.; Photo-induced negative differential resistance in a resistive switching memory device based on $BiFeO_3$/ZnO heterojunctions, *Applied Materials Today*, **2019**, 14, 21-28.
30. Wu, J.; Wang, J.; ZnO as a buffer layer for growth of $BiFeO_3$ thin films, *Journal of Applied Physics*, **2010**, 108, 034102.
31. Solanki, P.; Vala, M.; Dhruv, D.; Bhatt, S.V.; Kataria, B.; Resistive switching behaviour of novel $GdMnO_3$-based heterostructures, *Surfaces and Interfaces*, **2022**, 102474.
32. Negi, P.; Dixit, G.; Agrawal, H.M.; Kumar, H.; Srivastava, R.C.; Sati, P.C.; Gupta, V.; Asokan, K.; Tuning of structural and optical properties by sintering of multiferroic $GdMnO_3$ precursor, *Ferroelectrics*, **2017**, *519*, 200-208.
33. Mansouri, S.; Jandl, S.; Mukhin, A.; Ivanov, V.Y.; Balbashov, A.; A comparative raman study between $PrMnO_3$, $NdMnO_3$, $TbMnO_3$ and $DyMnO_3$, *Scientific Reports*, **2017**, *7*, 1–9.
34. Romaguera-Barcelay, Y.; Agostinho Moreira, J.; Almeida, A.; Tavares, P.B.; Pérez de la Cruz, J.; Structural, electrical and magnetic properties of magnetoelectric $GdMnO_3$ thin films prepared by a sol–gel method, *Thin Solid Films*, **2014**, *564*, 419-425.
35. Choithrani, R.; Rao, M.N.; Chaplot, S.; Gaur, N.; Singh, R.; Lattice dynamics of manganites RMnO3 (R= Sm, Eu or Gd): instabilities and coexistence of orthorhombic and hexagonal phases, *New Journal of Physics*, **2009**, 11, 073041.
36. Iliev, N.; Abrashev, M.; Lee, H.-G.; Popov, V.; Sun, Y.; Thomsen, C.; Meng, R.; Chu, C.; Raman active phonons in orthorhombic $YMnO_3$ and $LaMnO_3$, *Journal of Physics and Chemistry of Solids*, **1998**, 59, 1982-1984.
37. Merkulov, V.I.; Fox, J.R.; Li, H.-C.; Si, W.; Sirenko, A.; Xi, X.; Metal–oxide bilayer Raman scattering in $SrTiO_3$ thin films, *Applied Physics Letters*, **1998**, *72*, 3291-3293.
38. Soni, B.; Deshpande, M.; Bhatt, S.; Garg, N.; Chaki, S.; Studies on ZnO nanorods synthesized by hydrothermal method and their characterization, Журнал Нано-Та Електронної Фізики. **2013**, 04077–6.
39. Sarkar, S.; Patra, S.; Bera, S.; Paul, G.; Ghosh, R.; Rectifying properties of sol–gel synthesized Al: ZnO/Si (N–n) thin film heterojunctions, *Physica E: Low-Dimensional Systems and Nanostructures*, **2012**, *46*, 1–5.
40. Cui, Y.; Peng, H.; Wu, S.; Wang, R.; Wu, T.; Complementary Charge Trapping and Ionic Migration in Resistive Switching of Rare-Earth Manganite $TbMnO_3$, *ACS Appl. Mater. Interfaces*, **2013**, *5*, 1213-1217.
41. Huang, M.; Liang, J.; Zhang, P.; Li, Y.; Han, Y.; Yang, Z.; Pan, W.; Wan, C.; Opaque $Gd_2Zr_2O_7$/$GdMnO_3$ thermal barrier materials for thermal radiation shielding: The effect of polaron excitation, *Journal of Materials Science & Technology*, **2022**, *100*, 67-74.
42. Solanki, P.; Doshi, R.; Khachar, U.; Choudhary, R.; Kuberkar, D.; Thickness dependent transport and magnetotransport in CSD grown $La_{0.7}Pb_{0.3}MnO_3$ manganite films, *Materials Research Bulletin*, **2011**, 46, 1118-1123.
43. Salbego, P.R.; Orlando, T.; Farias, F.F.; Bonacorso, H.G.; Martins, M.A.; *Journal: European Journal of Organic Chemistry*, **2019**, *21*, 3464-3471, *European Journal of Organic Chemistry*, **2019**, 3464-3471.
44. Saravanakumar, B.; Mohan, R.; Kim, S.-J.; An investigation of the electrical properties of p-type Al: N Co-doped ZnO thin films, *Journal of the Korean Physical Society*, **2012**, *61*, 1737-1741.
45. Venkateshwarlu, D.; Dadhich, H.; Rajyaguru, B.; Hans, S.; Ranjan, M.; Venkatesh, R.; Ganesan, V.; Solanki, P.; Shah, N.; Semiconducting nature and magnetoresistance behaviour of ZnO/$La_{0.3}Ca_{0.7}MnO_3$/ $SrTiO_3$ heterostructures, *Materials Science in Semiconductor Processing*, **2021**, 136, 106154.
46. Sagapariya, K.; Venkateshwarlu, D.; Rajyaguru, B.; Gadani, K.; Shrimali, V.; Pandya, D.; Amaladass, E.; Shah, N.; Solanki, P.; Transport properties and electroresistance of manganite based heterostructure, *Ceramics International*, **2019**, *45*, 19456-19466.
47. Rajyaguru, B.; Boricha, H.; Shrimali, V.; Joshi, A.; Asokan, K.; Shah, N.; Solanki, P.; Fabrication and Characterization of Manganite Based p–n Junction, *Materials Today: Proceedings*, **2018**, *5*, 9927-9934.
48. Asghar, M.; Mahmood, K.; Rabia, S.; S.B. M, Shahid, M.Y.; Hasan, M.A.; Investigation of temperature dependent barrier height of Au/ZnO/Si schottky diodes, IOP Conf. Ser.: Mater. Sci. Eng., **2014**, 60, 012041.